

Direct evidence for the emergence of a pressure induced nodal superconducting gap in the iron-based superconductor

Ba_{0.65}Rb_{0.35}Fe₂As₂

Z. Guguchia,^{1,*} A. Amato,¹ J. Kang,² H. Luetkens,¹ P.K. Biswas,¹

G. Prando,³ F. von Rohr,⁴ Z. Bukowski,⁵ A. Shengelaya,⁶

H. Keller,⁴ E. Morenzoni,¹ R.M. Fernandes,² and R. Khasanov¹

¹*Laboratory for Muon Spin Spectroscopy,*

Paul Scherrer Institute, CH-5232 Villigen PSI, Switzerland

²*School of Physics & Astronomy, University of Minnesota, Minneapolis, MN 55455, USA*

³*Leibniz-Institut für Festkörper- und Werkstoffforschung*

(IFW) Dresden, D-01171 Dresden, Germany

⁴*Physik-Institut der Universität Zürich,*

Winterthurerstrasse 190, CH-8057 Zürich, Switzerland

⁵*Institute of Low Temperature and Structure Research,*

Polish Academy of Sciences, 50-422 Wrocław, Poland

⁶*Department of Physics, Tbilisi State University,*

Chavchavadze 3, GE-0128 Tbilisi, Georgia

Abstract

Identifying the superconducting (SC) gap structure of the iron-based high-temperature superconductors (Fe-HTS's) remains a key issue for the understanding of superconductivity in these materials. In contrast to other unconventional superconductors, in the Fe-HTS's both d -wave and extended s -wave pairing symmetries are close in energy, with the latter believed to be generally favored over the former. Probing the proximity between these very different SC states and identifying experimental parameters that can tune them, are of central interest. Here we report high-pressure muon spin rotation experiments on the temperature-dependent magnetic penetration depth $\lambda(T)$ in the optimally doped Fe-HTS $\text{Ba}_{0.65}\text{Rb}_{0.35}\text{Fe}_2\text{As}_2$. At ambient pressure this material is known to be a nodeless s -wave superconductor. Upon pressure a strong decrease of $\lambda(0)$ is observed, while the SC transition temperature remains nearly constant. More importantly, the low-temperature behavior of $1/\lambda^2(T)$ changes from exponential saturation at zero pressure to a power-law with increasing pressure, providing unambiguous evidence that hydrostatic pressure promotes nodal SC gaps. Comparison to microscopic models favors a d -wave over a nodal s^{+-} -wave pairing as the origin of the nodes. Our results provide a new route of understanding the complex topology of the SC gap in Fe-HTS's.

PACS numbers:

I. INTRODUCTION

After six years of intensive research on the Fe-based high temperature superconductors (Fe-HTS's), no consensus on a universal gap structure has been reached. There is evidence that small differences in electronic or structural properties can lead to a strong diversity in the superconducting (SC) gap structure. On the one hand, nodeless isotropic gap functions were observed in optimally doped $\text{Ba}_{1-x}\text{K}_x\text{Fe}_2\text{As}_2$, $\text{Ba}_{1-x}\text{Rb}_x\text{Fe}_2\text{As}_2$ and $\text{BaFe}_{2-x}\text{Ni}_x\text{As}_2$ as well as in $\text{BaFe}_{2-x}\text{Co}_x\text{As}_2$, $\text{K}_x\text{Fe}_{2-y}\text{Se}_2$, and $\text{FeTe}_{1-x}\text{Se}_x$ [1–8]. On the other hand, signatures of nodal SC gaps were reported in LaOFeP , LiFeP , KFe_2As_2 , $\text{BaFe}_2(\text{As}_{1-x}\text{P}_x)_2$, $\text{BaFe}_{2-x}\text{Ru}_x\text{As}_2$, FeSe as well as in over-doped $\text{Ba}_{1-x}\text{K}_x\text{Fe}_2\text{As}_2$ and $\text{BaFe}_{2-x}\text{Ni}_x\text{As}_2$ [7, 9–17]. Understanding what parameters of the systems control the different SC gap structures observed experimentally is paramount to elucidate the microscopic pairing mechanism in the Fe-HTS's and, more generally, to provide a deeper understanding of the phenomenon of high-temperature superconductivity. On the theoretical front, it has been proposed that both the s^{+-} -wave and d -wave states are close competitors for the SC ground state [18–24]. Although the former generally wins, it has been pointed out that a d -wave state may be realized upon removing electron or hole pockets. On the experimental front, a sub-leading d -wave collective mode was observed by Raman experiments inside the fully gapped SC state of optimally doped $\text{Ba}_{1-x}\text{K}_x\text{Fe}_2\text{As}_2$ [25, 26]. In KFe_2As_2 , a change of the SC pairing symmetry by hydrostatic pressure has been recently proposed, based on the V -shaped pressure dependence of T_c [27]. However, no direct experimental evidence for a pressure induced change of either the SC gap symmetry or the SC gap structure in the Fe-HTS's has been reported until now. Here, we show unambiguous evidence for the appearance of SC nodes in optimally-doped $\text{Ba}_{1-x}\text{Rb}_x\text{Fe}_2\text{As}_2$ upon applied pressure, consistent with a change from a nodeless s^{+-} -wave state to either a nodal s^{+-} -wave or a d -wave state.

Our results rely on measurements of the magnetic penetration depth λ , which is one of the fundamental parameters of a superconductor, since it is related to the superfluid density n_s via $1/\lambda^2 = \mu_0 e^2 n_s / m^*$ (where m^* is the effective mass). Most importantly, the temperature dependence of λ is particularly sensitive to the presence of SC nodes: while in a fully gapped SC $\Delta\lambda^{-2}(T) \equiv \lambda^{-2}(0) - \lambda^{-2}(T)$ vanishes exponentially at low T , in a nodal SC it vanishes as a power of T . The muon-spin rotation (μSR) technique provides a powerful tool to measure λ in type II superconductors [28]. A μSR experiment in the vortex

state of a type II superconductor allows the determination of λ in the bulk of the sample, in contrast to many techniques that probe λ only near the surface.

For the compound $\text{Ba}_{0.65}\text{Rb}_{0.35}\text{Fe}_2\text{As}_2$ investigated here, and for the closely related system $\text{Ba}_{1-x}\text{K}_x\text{Fe}_2\text{As}_2$, previous μSR measurements of $\lambda(T)$ revealed a nodeless multi-gap SC state [2, 3], in agreement with ARPES measurements [1, 29, 30]. In this communication, we report on μSR studies of $\lambda(0)$ and of the temperature dependence of $\Delta\lambda^{-2}$ in optimally doped $\text{Ba}_{0.65}\text{Rb}_{0.35}\text{Fe}_2\text{As}_2$ under hydrostatic pressures. This system exhibits the highest $T_c \simeq 37$ K among the extensively studied “122” family of Fe-HTS’s. We observe that while T_c stays nearly constant upon application of pressure, $\lambda(0)$ decreases substantially. In view of previous works in another “122” compound that reported a sharp peak of $\lambda(0)$ at a quantum critical point [31], we interpret the observed suppression of $\lambda(0)$ as evidence that pressure moves the system away from a putative quantum critical point in $\text{Ba}_{0.65}\text{Rb}_{0.35}\text{Fe}_2\text{As}_2$. More importantly, we find a qualitative change in the low-temperature behavior of $\Delta\lambda^{-2}(T)$ as pressure is increased. While at $p = 0$ an exponential suppression characteristic of a nodeless superconductivity is observed, for $p = 2.25$ GPa a clear power-law behavior is found. Because pressure does not affect the impurity concentration, which could promote power-law behavior even for a nodeless system [32], our findings provide strong evidence for a nodeless to nodal SC transition. Our fittings to microscopic models reveal that this behavior is more compatible with a d -wave state rather than an s^{+-} state with accidental nodes, indicating that pressure promotes a change in the pairing symmetry.

II. RESULTS

A. Probing the nonuniform field distribution in the vortex state under pressure

Figures 1a and b exhibit the transverse-field (TF) μSR -time spectra for $\text{Ba}_{0.65}\text{Rb}_{0.35}\text{Fe}_2\text{As}_2$, measured at ambient $p = 0$ GPa and maximum applied pressure $p = 2.25$ GPa, respectively. The spectra above (45 K) and below (1.7 K) the SC transition temperature T_c are shown. Above T_c the oscillations show a small relaxation due to the random local fields from the nuclear magnetic moments. Below T_c the relaxation rate strongly increases with decreasing temperature due to the presence of a nonuniform local magnetic field distribution as a result of the formation of a flux-line lattice (FLL) in the SC state.

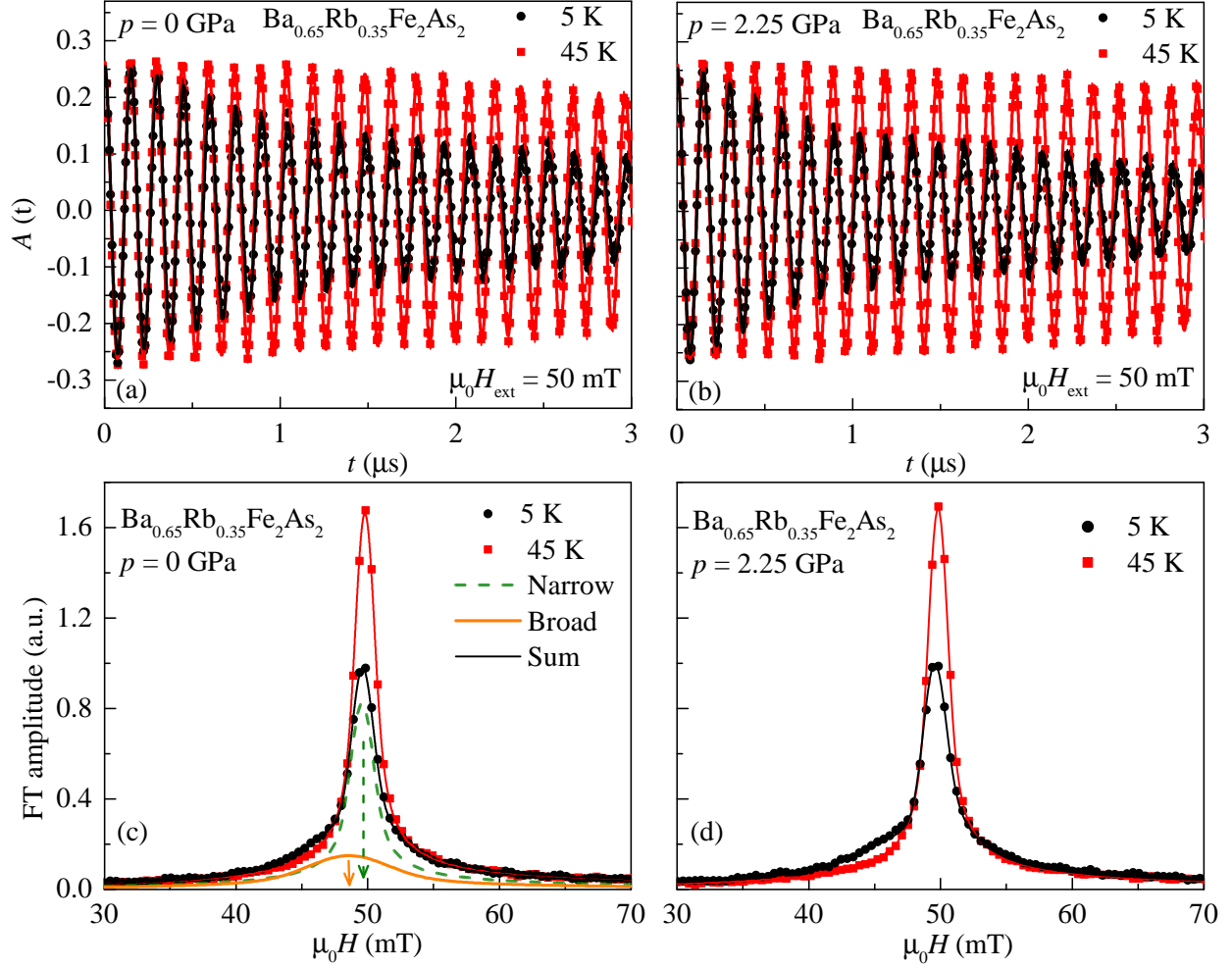


Figure 1: (Color online) **Transverse-field (TF) μ SR time spectra and the corresponding Fourier transforms (FT's) of $\text{Ba}_{0.65}\text{Rb}_{0.35}\text{Fe}_2\text{As}_2$.** The spectra are obtained above (45 K) and below (5 K) T_c (after field cooling the sample from above T_c): (a,c) $p = 0$ GPa and (b,d) $p = 2.22$ GPa. The solid lines in panels a and b represent fits to the data by means of Eq. 3. The solid lines in panels c and d are the FT's of the fitted time spectra. The dashed and solid arrows indicate the first moments for the signals of the pressure cell and the sample, respectively.

Figures 1c and d show the Fourier transforms (FT's) of the μ SR time spectra shown in Figs. 1a and b, respectively. At $T = 5$ K the narrow signal around $\mu_0 H_{\text{ext}} = 50$ mT (see Figs. 1c and d) originates from the pressure cell, while the broad signal with a first moment $\mu_0 H_{\text{int}} < \mu_0 H_{\text{ext}}$, marked by the solid arrow in Fig. 1c, arises from the SC sample.

Below T_c a large diamagnetic shift of $\mu_0 H_{\text{int}}$ experienced by the muons is observed at all applied pressures. This is evident in Fig. 2a, where we plot the temperature dependence of

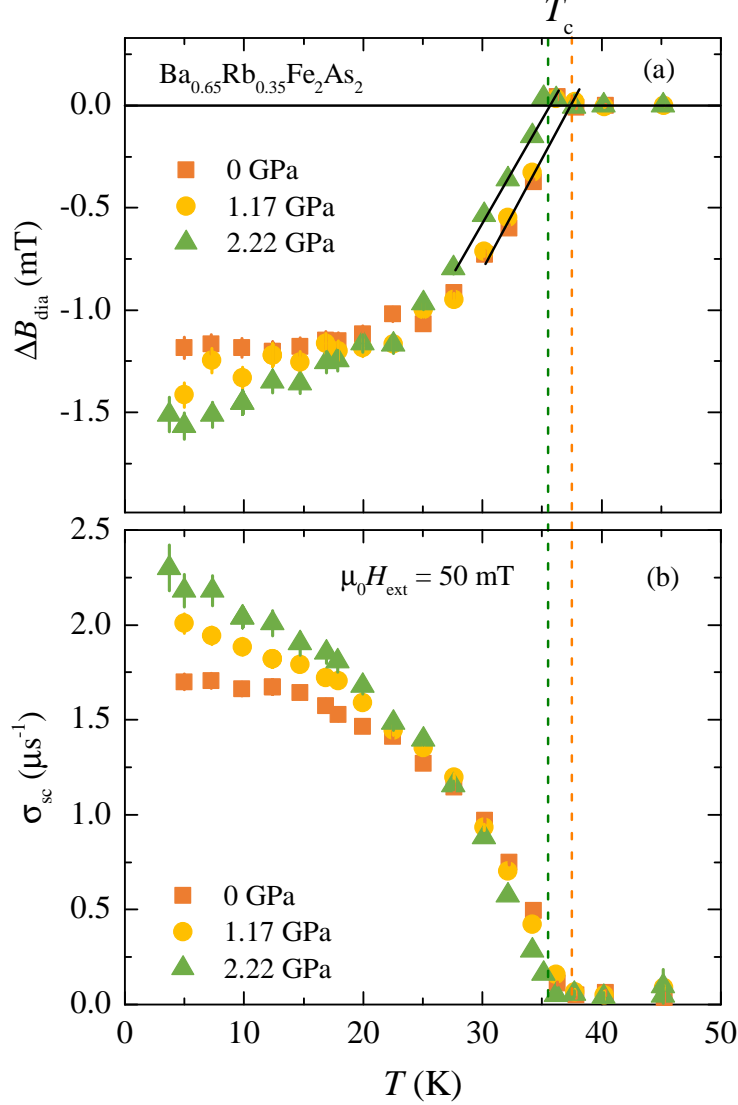


Figure 2: (Color online) **Diamagnetic shift ΔB_{dia} (a) and the muon spin relaxation rate σ_{sc} (b) of $\text{Ba}_{0.65}\text{Rb}_{0.35}\text{Fe}_2\text{As}_2$ as a function of temperature at various pressures.** (a) The definition of the diamagnetic shift ΔB_{dia} is given in the text. (b) The muon spin relaxation rate σ_{sc} is measured in a magnetic field of $\mu_0 H = 50$ mT. The dashed vertical lines denote T_c for $p = 0$ and 2.22 GPa.

the diamagnetic shift $\Delta B_{\text{dia}} = \mu_0[H_{\text{int,SC}} - H_{\text{int,NS}}]$ for $\text{Ba}_{0.65}\text{Rb}_{0.35}\text{Fe}_2\text{As}_2$ at various pressures, where $\mu_0 H_{\text{int,SC}}$ denotes the internal field measured in the SC state and $\mu_0 H_{\text{int,NS}}$ the internal field measured in the normal state at 45 K. Note, that $\mu_0 H_{\text{int,NS}}$ is temperature independent. This diamagnetic shift indicates the bulk character of superconductivity and excludes the possibility of field induced magnetism [33] in $\text{Ba}_{0.65}\text{Rb}_{0.35}\text{Fe}_2\text{As}_2$ at all applied pressures. The

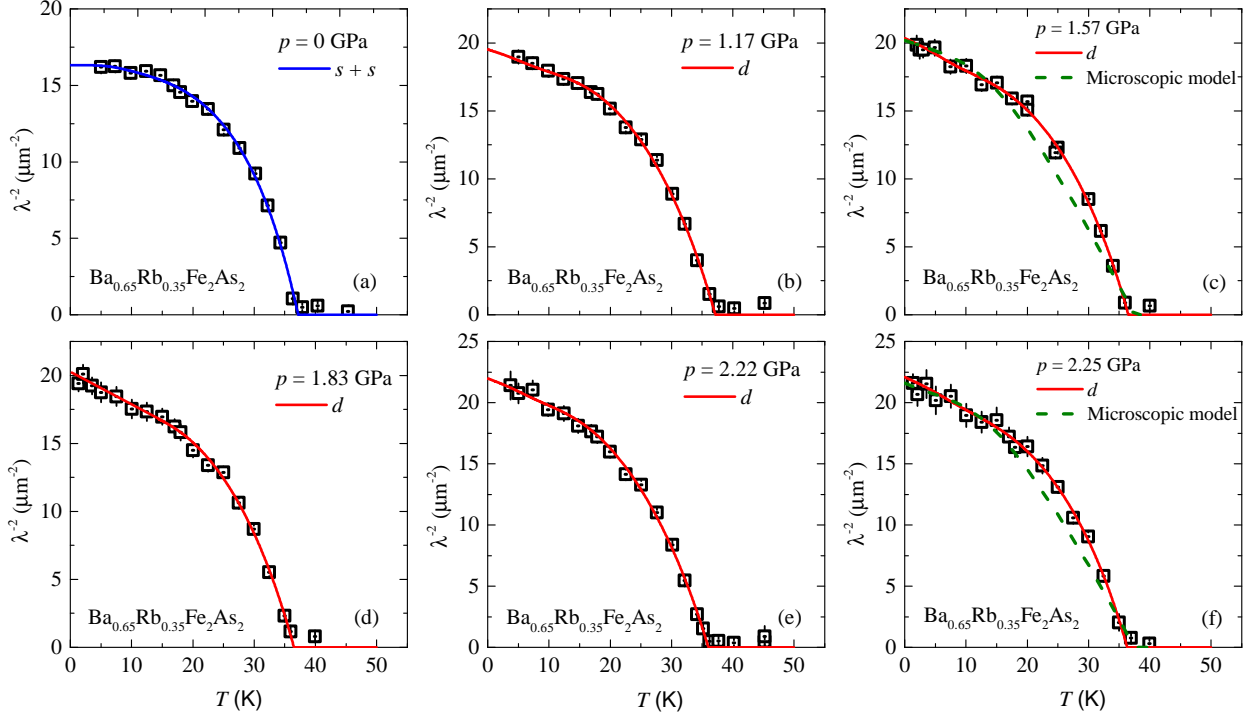


Figure 3: (Color online) **Pressure evolution of $\lambda^{-2}(T)$ of $\text{Ba}_{0.65}\text{Rb}_{0.35}\text{Fe}_2\text{As}_2$.** The temperature dependence of λ^{-2} measured at various applied hydrostatic pressures for $\text{Ba}_{0.65}\text{Rb}_{0.35}\text{Fe}_2\text{As}_2$. The solid line for $p = 0$ GPa corresponds to a two-gap s -wave model (a) and the solid lines for finite pressure represent a fits to the data using a multiband d -wave model (b-f). The dashed lines in panels (c) and (f) represent fits to the data using the microscopic model described in the supplemental material.

SC transition temperature T_c is determined from the intercept of the linearly extrapolated ΔB_{dia} curve its zero line (we used the same criterium for determination of T_c from $\Delta B_{\text{dia}}(T)$ as from the susceptibility data $\chi_m(T)$, presented in the supplementary material). It is found to be $T_c = 36.9(7)$ K and $35.9(5)$ K for $p = 0$ GPa and 2.25 GPa, respectively. The ambient pressure value of T_c is in perfect agreement with $T_c = 36.8(5)$ K obtained from susceptibility and specific heat measurements (see supplemental material). At the highest pressure of $p = 2.25$ GPa applied, T_c decreases only by $\simeq 1$ K, indicating only a small pressure effect on T_c in $\text{Ba}_{0.65}\text{Rb}_{0.35}\text{Fe}_2\text{As}_2$. The temperature dependence of the muon spin depolarization rate σ_{sc} , which is proportional to the second moment of the field distribution (the moments of the field distribution probed by the muons were extracted with the equations described in the Method section), of $\text{Ba}_{0.65}\text{Rb}_{0.35}\text{Fe}_2\text{As}_2$ in the SC state at selected pressures is shown

in Fig. 2b. Below T_c the relaxation rate σ_{sc} starts to increase from zero with decreasing temperature due to the formation of the FLL. It is interesting that the low-temperature value $\sigma_{sc}(5\text{ K})$ increases substantially under pressure (see Fig. 2b): $\sigma_{sc}(5\text{ K})$ increases about 30 % from $p = 0\text{ GPa}$ to $p = 2.25\text{ GPa}$. Interestingly, the form of the temperature dependence of σ_{sc} , which reflects the topology of the SC gap, changes as a function of pressure. The most striking change is in the low-temperature behaviour of $\sigma_{sc}(T)$. At ambient pressure $\sigma_{sc}(T)$ shows a flat behavior below $T/T_c \simeq 0.4$, whereas the high-pressure data exhibit a steeper (linear) temperature dependence of $\sigma_{sc}(T)$ below $T/T_c \simeq 0.4$. We show in the following how these behaviors indicate the appearance of nodes in the gap function.

B. Temperature and pressure dependent magnetic penetration depth

In order to investigate a possible change of the symmetry of the SC gap, we note that $\lambda(T)$ is related to the relaxation rate $\sigma_{sc}(T)$ by the equation [34]:

$$\frac{\sigma_{sc}(T)}{\gamma_\mu} = 0.06091 \frac{\Phi_0}{\lambda^2(T)}, \quad (1)$$

where γ_μ is the gyromagnetic ratio of the muon, and Φ_0 is the magnetic-flux quantum. Thus, the flat T -dependence of σ_{sc} observed at $p = 0$ for low temperatures (see Fig. 2b) is consistent with a nodeless superconductor, in which $\lambda^{-2}(T)$ reaches its zero-temperature value exponentially. On the other hand, the linear T -dependence of σ_{sc} observed at $p = 2.25\text{ GPa}$ (see Fig. 2b) indicates that $\lambda^{-2}(T)$ reaches $\lambda^{-2}(0)$ linearly which is characteristic of line nodes. This is the most striking result of this communication: Pressure in an optimally-doped Fe-HTS can tune a nodeless gap into a nodal gap. Although this qualitative analysis is robust, it does not elucidate whether these nodes arise due to a nodal s^{+-} state or a d -wave state.

To proceed with a quantitative analysis, we consider the local (London) approximation ($\lambda \gg \xi$, where ξ is the coherence length) and first employ the empirical α -model. The latter, widely used in previous investigations of the penetration depth of multi-band superconductors [3, 35–40], assumes that the gaps occurring in different bands, besides a common T_c , are independent of each other. Then, the superfluid density is calculated for each component separately [3] and added together with a weighting factor. For our purposes, a two-band

model suffices, yielding:

$$\frac{\lambda^{-2}(T)}{\lambda^{-2}(0)} = \omega_1 \frac{\lambda^{-2}(T, \Delta_{0,1})}{\lambda^{-2}(0, \Delta_{0,1})} + \omega_2 \frac{\lambda^{-2}(T, \Delta_{0,2})}{\lambda^{-2}(0, \Delta_{0,2})}, \quad (2)$$

where $\lambda(0)$ is the penetration depth at zero temperature, $\Delta_{0,i}$ is the value of the i -th SC gap ($i = 1, 2$) at $T = 0$ K, and ω_i is the weighting factor which measures their relative contributions to λ^{-2} (i.e. $\omega_1 + \omega_2 = 1$).

The results of this analysis are presented in Figs. 3a-f, where the temperature dependence of λ^{-2} for $\text{Ba}_{0.65}\text{Rb}_{0.35}\text{Fe}_2\text{As}_2$ is plotted at various pressures. We consider two different possibilities for the gap functions: either a constant gap, $\Delta_{0,i} = \Delta_i$, or an angle-dependent gap of the form $\Delta_{0,i} = \Delta_i \cos 2\varphi$, where φ is the polar angle around the Fermi surface. The data at $p = 0$ GPa are described remarkably well by two constant gaps, $\Delta_1 = 2.7(5)$ meV and $\Delta_2 = 8.4(3)$ meV. These values are in perfect agreement with our previous results [3] and also with ARPES experiments [29], pointing out that most Fe-based HTS's exhibit two-gap behavior, characterized by one large gap with $2\Delta_2/k_B T_c = 7(2)$ and one small gap with $2\Delta_1/k_B T_c = 2.5(1.5)$. In contrast to the case $p = 0$ GPa, for all applied pressures $\lambda^{-2}(T)$ is better described by one constant gap and one angle-dependent gap, confirming the presence of gap nodes, as inferred from our qualitative analysis. Note that a fitting to two angle-dependent gaps is inconsistent with the data.

To understand the implications of the fitting to a constant and an angle-dependent gap for finite pressures, we analyze the two different scenarios in which nodes can emerge: a nodal s^{+-} state (with gap functions of different signs in the hole and in the electron pockets) and a d -wave state. In the former, the position of the nodes are accidental, i.e. not enforced by symmetry, while in the latter the nodes are enforced by symmetry to be on the Brillouin zone diagonals. Schematic representations of both scenarios are shown in Fig. 4, where a density plot of the gap functions is superimposed to the typical Fermi surface of the iron pnictides, consisting of one or more hole pockets at the center of the Brillouin zone, and electron pockets at the border of the Brillouin zone. In this figure, we set the accidental nodes of the s^{+-} state to be on the electron pockets, as observed by ARPES in the related compound $\text{BaFe}_2(\text{As}_{1-x}\text{P}_x)_2$ [17]. Note that in the d -wave state, while nodes appear in the hole pockets, the electron pockets have nearly uniform gaps. Thus, the fact that the fitting to the α -model gives a constant and an angle-dependent gap is consistent with a d -wave state.

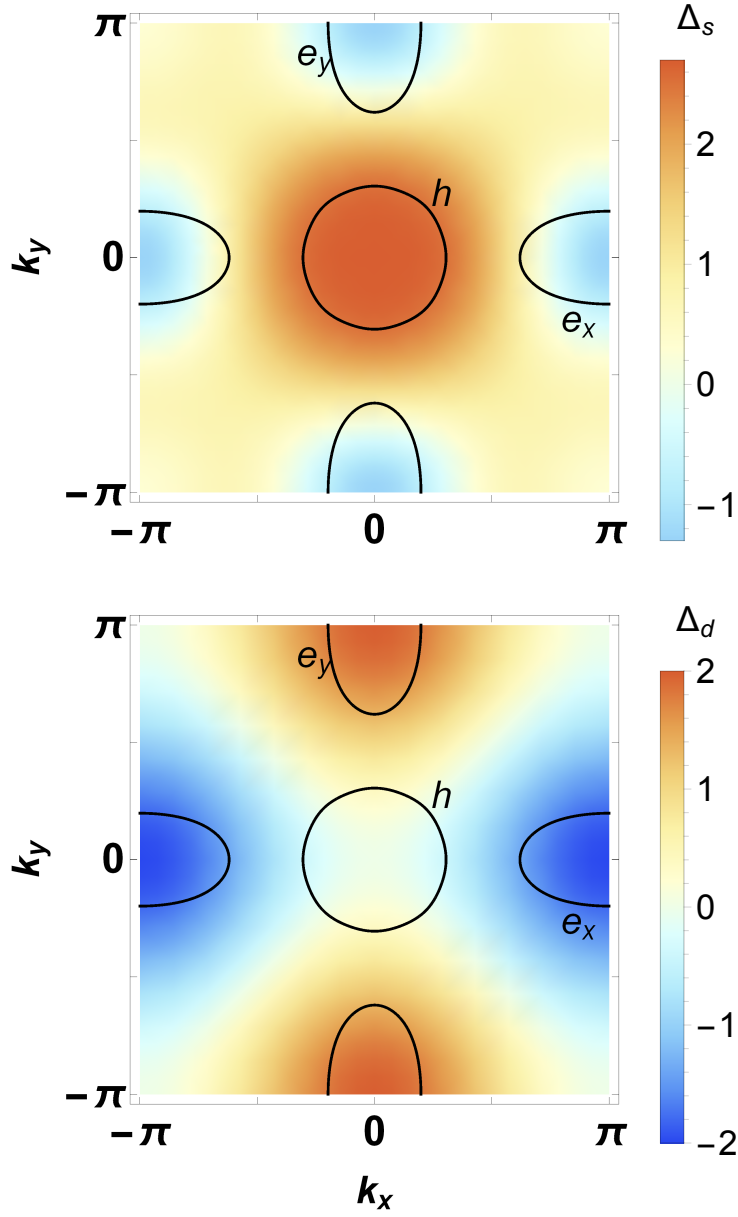


Figure 4: **Schematic representation of the nodal s^{+-} and d -wave states.** In both panels, a density plot of the gap function is superimposed to a representative Fermi surface consisting of a hole pocket (h) at the center and an electron pocket (e) at the borders of the Brillouin zone. In the nodal s^{+-} states (upper panel), the nodes are not enforced by symmetry (here they are located at the electron pockets). In the d -wave state (lower panel), the nodes are enforced by symmetry to be on the diagonals of the Brillouin zone, and therefore can only cross the hole pockets.

To contrast the scenarios of a nodal s^{+-} gap and a d -wave gap, we consider a microscopic model that goes beyond the simplifications of independent gap functions of the α -model discussed above. In this microscopic model, the fully coupled non-linear gap equations are solved for a hole pocket h and two electron pockets $e_{1,2}$, and the penetration depth is calculated at all temperatures. The free parameters are then the density of states of the pockets, the amplitude of the pairing interaction, and the gap functions themselves (details in the supplementary material). For simplicity, the anisotropies of the electron pockets are neglected, the Fermi velocities of the pockets are assumed to be nearly the same, and the gaps are expanded in their leading harmonics. Thus, for the nodal s^{+-} state we have $\Delta_h = \Delta_{h,0}$ and $\Delta_{e_i} = \Delta_{e,0} (r \pm \cos 2\varphi_e)$, whereas for the d -wave state it follows that $\Delta_h = \Delta_{h,0} \cos 2\varphi_h$ and $\Delta_{e_i} = \pm \Delta_{e,0}$. Note the difference in the position of the nodes in each case: while for the d -wave case they are always at $\varphi_h = \pm\pi/4$, for the nodal s^{+-} the nodes exist only when $r < 1$ at arbitrary positions $\varphi_e = \pm\frac{1}{2} \arccos r$. The results of the fittings for the pressures $p = 1.57$ GPa and $p = 2.25$ GPa imposing a nodal s^{+-} state are shown in Figs. 3c and f. Remarkably, we find in both cases that the best fit gives $r \rightarrow 0$. This extreme case is, within our model, indistinguishable from the fitting to the d -wave state, since in both cases the nodes are at $\varphi = \pm\pi/4$ (albeit in different Fermi pockets). We note that from the fits one cannot completely rule out the possibility of small but non-vanishing values of r . Therefore, at least within our model, a nodal s^{+-} state is compatible with the data only if the accidental nodes are fine-tuned to lie either at or very close to the diagonals of the electron pockets for a broad pressure range. Since the position of the accidental nodes is expected to be sensitive to the topology of the Fermi surface, and consequently to pressure, it seems more plausible that the gap state is d -wave, since in that case the position of the gaps is enforced by symmetry to be along the diagonals of the hole pockets regardless of the value of the pressure.

The pressure dependence of all the parameters extracted from the data analysis within the α model are plotted in Figs. 5(a-c). From Fig. 5a a substantial decrease of $\lambda(0)$ with pressure is evident. At the maximum applied pressure of $p = 2.25$ GPa the reduction of $\lambda(0)$ is approximately 15 % compared to the value at $p = 0$ GPa. Both Δ_1 and Δ_2 show a small reduction upon increasing the pressure from $p = 0$ to 1.17 GPa, while above $p = 1.17$ GPa the gaps values stay constant. On the other hand, the relative contribution ω_2 of the small gap to the superfluid density increases by approximately factor of 2 for the

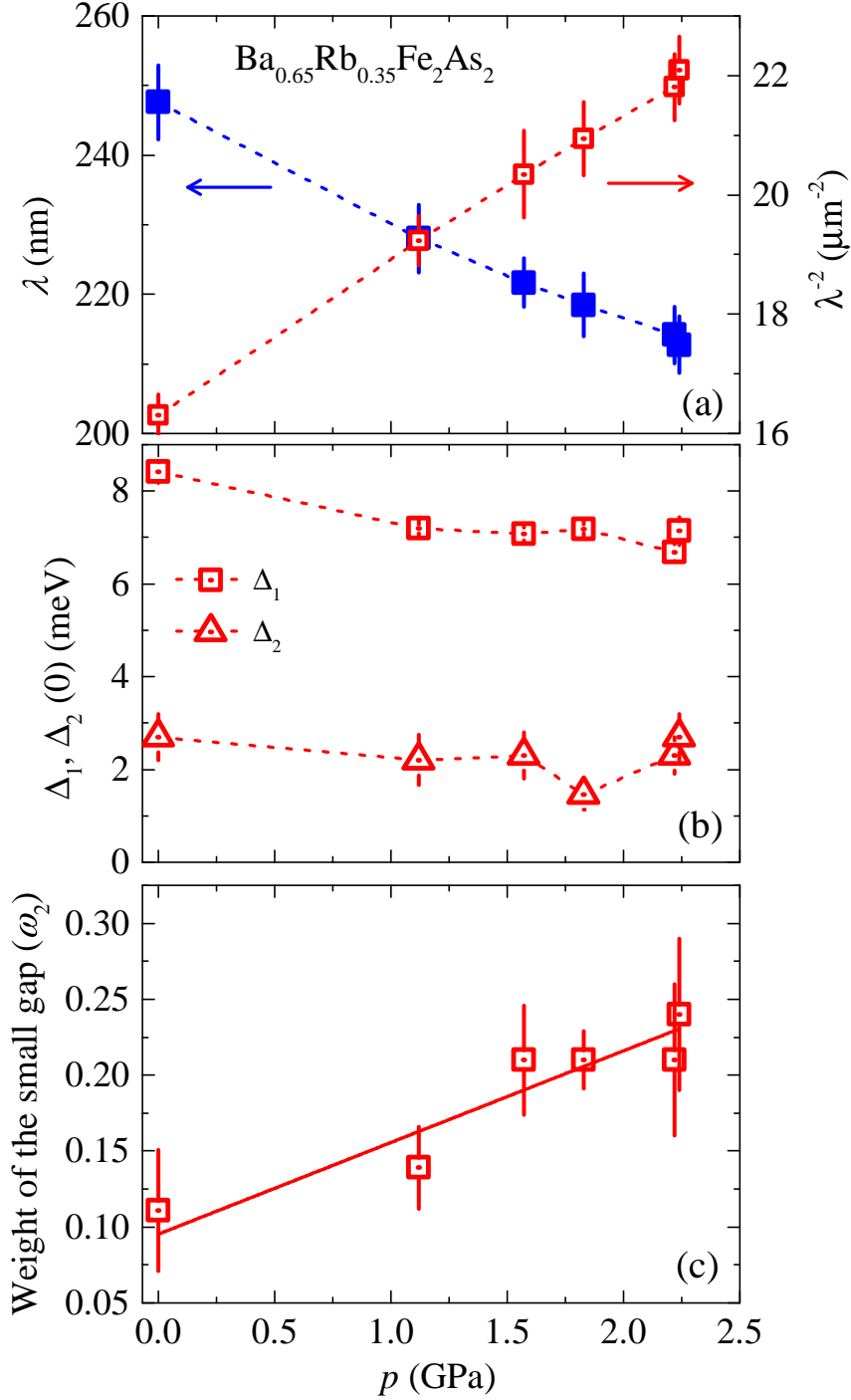


Figure 5: (Color online) **Pressure dependence of various quantities of $\text{Ba}_{0.65}\text{Rb}_{0.35}\text{Fe}_2\text{As}_2$.** (a) The magnetic penetration depth $\lambda(0)$ and $\lambda^{-2}(0)$. (b) The zero-temperature gap values $\Delta_{1,2}(0)$. The relative weight ω_2 of the small gap to the superfluid density. The dashed lines are guides to the eyes, and the solid lines represent linear fits to the data.

maximum applied pressure of $p = 2.25$ GPa (see Fig. 5c), indicating a spectral weight shift to the smaller gap. The parameters extracted from the microscopic model are discussed in

the supplementary material.

III. DISCUSSION

The most essential finding of our paper is the observation that pressure promotes a nodal SC gap in $\text{Ba}_{0.65}\text{Rb}_{0.35}\text{Fe}_2\text{As}_2$. This conclusion is robust and model-independent, as it relies on the qualitative change in the low-temperature behavior of $\Delta\lambda^{-2}$ from exponential to linear in T upon applied pressure. To our knowledge this is the first direct experimental demonstration of a pressure induced change in the superconducting gap structure in a Fe-HTS's. Two possible gap structures could be realized at finite pressures: a nodal s^{+-} state and a d -wave state. In the first case, the change from nodeless s^{+-} to nodal s^{+-} is a crossover rather than a phase transition [41, 42], whereas in the latter it is an actual phase transition that could harbor exotic pairing states, such as $s + id$ [21–23] or $s + d$ [43].

Additional results provide important clues of how pressure may induce either an s^{+-} or a d -wave state. In the closely related optimally-doped compound $\text{Ba}_{0.6}\text{K}_{0.4}\text{Fe}_2\text{As}_2$, Raman spectroscopy [26], as well as theoretical calculations [20, 21], reveal a sub-dominant d -wave state close in energy to the dominant s^{+-} state. Pressure may affect this intricate balance, and tip the balance in favor of the d -wave state. On the other hand, theoretical calculations have shown that the pnictogen height is an important factor in determining the structure of the s^{+-} SC order parameter [18]. A systematic comparison of the quasiparticle excitations in the 1111, 122, and 111 families of Fe-HTS's showed that the nodal s^{+-} state is favored when the pnictogen height decreases below a threshold value of $\simeq 1.33 \text{ \AA}$ [44]. Hydrostatic pressure may indeed shorten the pnictogen height and consequently modify the s^{+-} gap structure from nodeless to nodal. Although our fitting of the penetration depth data to both a microscopic model and an effective α -model suggest that the d -wave state is more likely to be realized than the nodal s^{+-} state, further quantitative calculations of the pressure effect are desirable to completely discard a nodal s^{+-} state.

Besides the appearance of nodes with pressure, another interesting observation is the reduction of $\lambda(0)$ under pressure, despite the fact that T_c remains nearly unchanged. Interestingly, in the compound $\text{BaFe}_2\text{As}_{2-x}\text{P}_x$, a sharp enhancement of $\lambda(0)$ is observed as optimal doping is approached from the overdoped side [31], which has been interpreted in terms of a putative quantum critical point (QCP) inside the SC dome [45–47]. In $\text{Ba}_{0.65}\text{Rb}_{0.35}\text{Fe}_2\text{As}_2$,

if such a putative QCP is also present, pressure is likely to move the system away from the putative QCP, which, according to the results of $\text{BaFe}_2\text{As}_{2-x}\text{P}_x$, would explain the observed suppression of the penetration depth at $T = 0$. This scenario does not explain why T_c stays nearly constant under pressure, but this could be due to the intrinsic flatness of T_c around optimal doping in $\text{Ba}_{1-x}\text{Rb}_x\text{Fe}_2\text{As}_2$. Note that a similar behavior for $\lambda(0)$ and T_c with pressure has been recently observed in $\text{LaFeAsO}_{1-x}\text{F}_x$ [48], but interpreted in terms of the interplay between impurity scattering and pressure. To distinguish unambiguously between these two scenarios, pressure-dependent studies of the quasiparticle mass in $\text{Ba}_{0.65}\text{Rb}_{0.35}\text{Fe}_2\text{As}_2$ are desirable, in order to probe whether a putative QCP is present or not in this compound.

IV. CONCLUSIONS

In conclusion, the zero-temperature magnetic penetration depth $\lambda(0)$ and the temperature dependence of λ^{-2} were studied in optimally doped $\text{Ba}_{0.65}\text{Rb}_{0.35}\text{Fe}_2\text{As}_2$ by means of μSR experiments as a function of pressure up to $p \simeq 2.25$ GPa. The SC transition temperature stays nearly constant under pressure, whereas a strong reduction of $\lambda(0)$ is observed, possibly related to the presence of a putative quantum critical point. Our main result is the demonstration that in the investigated Fe-based superconductor a nodal SC gap is promoted by hydrostatic pressure. Model calculations favor a d -wave over a nodal s^{+-} -wave pairing as the origin for the nodal gap. The present results offer important benchmarks for the elucidation of the complex microscopic mechanism responsible for the observed non-universality of the SC gap structure and of high-temperature superconductivity in the Fe-HTS's in general.

V. METHODS

Sample: Polycrystalline samples of $\text{Ba}_{0.65}\text{Rb}_{0.35}\text{Fe}_2\text{As}_2$ were prepared in evacuated quartz ampoules by a solid state reaction method. Fe_2As , BaAs , and RbAs were obtained by reacting high purity As (99.999 %), Fe (99.9%), Ba (99.9%), and Rb (99.95%) at 800 °C, 650 °C and 500 °C, respectively. Using stoichiometric amounts of BaAs or RbAs and Fe_2As , the terminal compounds BaFe_2As_2 and RbFe_2As_2 were synthesized at 950 °C and 650 °C, respectively. Finally, samples of $\text{Ba}_{1-x}\text{Rb}_x\text{Fe}_2\text{As}_2$ with $x = 0.35$ were prepared from appropriate amounts of single-phase BaFe_2As_2 and RbFe_2As_2 . The components were mixed,

pressed into pellets, placed into alumina crucibles, and annealed for 100 hours under vacuum at 650 °C with one intermittent grinding. Powder X-ray diffraction analysis revealed that the synthesized samples are single phase materials.

Pressure cell: Pressures up to 2.4 GPa were generated in a double wall piston-cylinder type of cell made of MP35N material, especially designed to perform μ SR experiments under pressure [49, 50]. As a pressure transmitting medium Daphne oil was used. The pressure was measured by tracking the SC transition of a very small indium plate by AC susceptibility. The filling factor of the pressure cell was maximized. The fraction of the muons stopping in the sample was approximately 40 %.

μ SR experiment: The measurements were performed using high-pressure μ SR technique, where an intense high-energy ($p_\mu = 100$ MeV/c) beam of muons is implanted in the sample through the pressure cell. In a μ SR experiment nearly 100 % spin-polarized muons μ^+ are implanted into the sample one at a time. The positively charged μ^+ thermalize at interstitial lattice sites, where they act as magnetic microprobes. In a magnetic material the muon spin precesses in the local field B_μ at the muon site with the Larmor frequency $\nu_\mu = \gamma_\mu/(2\pi)B_\mu$ (muon gyromagnetic ratio $\gamma_\mu/(2\pi) = 135.5$ MHz T⁻¹). By means of μ SR important length scale of superconductor can be measured, namely the magnetic penetration depth λ . When a type II superconductor is cooled below T_c in an applied magnetic field ranging between the lower (H_{c1}) and the upper (H_{c2}) critical field, a vortex lattice is formed which in general is incommensurate with the crystal lattice, and the vortex cores will be separated by much larger distances than those of the unit cell. Because the implanted muons stop at given crystallographic sites, they will randomly probe the field distribution of the vortex lattice. Such measurements need to be performed in a field applied perpendicular to the initial muon spin polarization (so called TF configuration).

Analysis of TF- μ SR data: Our zero-field μ SR experiments (see supplemental material) reveal a magnetic fraction of about 10 % in the sample, caused by the presence of diluted Fe moments as discussed in previous μ SR studies. The signal from the magnetically ordered parts vanishes within the first 0.2 μ s. Thus, the fits of TF data were restricted to times $t > 0.2$ μ s for all temperatures.

The TF μ SR data were analyzed by using the following functional form:[35]

$$P(t) = A_s \exp \left[- \frac{(\sigma_{sc}^2 + \sigma_{nm}^2)t^2}{2} \right] \cos(\gamma_\mu B_{int,s}t + \varphi) + A_{pc} \exp \left[- \frac{\sigma_{pc}^2 t^2}{2} \right] \cos(\gamma_\mu B_{int,pc}t + \varphi), \quad (3)$$

and A_{pc} denote the initial assymetries of the sample and the pressure cell, respectively. $\gamma/(2\pi) \simeq 135.5$ MHz/T is the muon gyromagnetic ratio, φ is the initial phase of the muon-spin ensemble, and B_{int} represents the internal magnetic field at the muon site. The relaxation rates σ_{sc} and σ_{nm} characterize the damping due to the formation of the vortex lattice in the SC state and of the nuclear magnetic dipolar contribution, respectively. In the analysis σ_{nm} was assumed to be constant over the entire temperature range and was fixed to the value obtained above T_c , where only nuclear magnetic moments contribute to the muon relaxation rate σ . The Gaussian relaxation rate σ_{pc} reflects the depolarization due to the nuclear magnetism of the pressure cell. It can be seen from the FT's shown in Figs. 1c and d that the width of the pressure cell signal increases below T_c . As shown previously [51], this is due to the influence of the diamagnetic moment of the SC sample on the pressure cell, leading to a temperature dependent σ_{pc} below T_c . In order to consider this influence, we assume a linear coupling between σ_{pc} and the field shift of the internal magnetic field in the SC state: $\sigma_{pc}(T) = \sigma_{pc}(T > T_c) + C(T)(\mu_0 H_{int,NS} - \mu_0 H_{int,SC})$, where $\sigma_{pc}(T > T_c) = 0.35 \mu s^{-1}$ is the temperature independent Gaussian relaxation rate. $\mu_0 H_{int,NS}$ and $\mu_0 H_{int,SC}$ are the internal magnetic fields measured in the normal and in the SC state, respectively. As indicated by the solid lines in Figs. 1a-d, the μ SR data are well described by Eq. (1). The solid lines in panels c and d are the FTs of the fitted curves shown in Figs. 1a and b. The model used describes the data rather well.

VI. ACKNOWLEDGMENTS

Experimental work was performed at the Swiss Muon Source (S μ S) Paul Scherrer Institute, Villigen, Switzerland. Z.G. acknowledge the support by the Swiss National Science Foundation. R.M.F and J.K. were support by the U.S. Department of Energy, Office of Science, Basic Energy Sciences, under award number de-sc0012336. A.S. acknowledges support from the SCOPES grant No. IZ74Z0-137322. G.P. is supported by the Humboldt Research

Fellowship for Postdoctoral Researchers.

VII. CONTRIBUTIONS

Project planning: Z.G.; Sample growth: Z.B.; μ SR experiments: Z.G.; R.K.; A.A.; H.L.; P.K.B.; E.M.; A.S.; G.P.; H.K., and F.V.R.; Magnetization experiment: Z.G., and F.V.R.; μ SR data analysis: Z.G.; Analysis of the penetration depth data with α -model: Z.G.; Analysis of the penetration depth data with the microscopic model: J.K., and R.M.F.; Data interpretation: Z.G.; R.M.F., and R.K.; Draft writing: Z.G., with contributions and/or comments from all authors.

* Electronic address: zurab.guguchia@psi.ch

- [1] Ding, H., Richard, P., Nakayama, K., Sugawara, T., Arakane, T., Sekiba, Y., Takayama, A., Souma, S., Sato, T., Takahashi, T., Wang, Z., Dai, X., Fang, Z., Chen, G.F., Luo, J.L. and Wang N.L. Observation of Fermi-surface-dependent nodeless superconducting gaps in $\text{Ba}_{0.6}\text{K}_{0.4}\text{Fe}_2\text{As}_2$. *Europhys. Lett.* **83**, 47001 (2008).
- [2] Khasanov, R., Evtushinsky, D.V., Amato, A., Klauss, H.-H., Luetkens, H., Niedermayer, Ch., Büchner, B., Sun, G.L., Lin, C.T., Park, J.T., Inosov, D.S. and Hinkov, V. Two-Gap Superconductivity in $\text{Ba}_{1-x}\text{K}_x\text{Fe}_2\text{As}_2$: A Complementary Study of the Magnetic Penetration Depth by Muon-Spin Rotation and Angle-Resolved Photoemission. *Phys. Rev. Lett.* **102**, 187005 (2009).
- [3] Guguchia, Z., Shermadini, Z., Amato, A., Maisuradze, A., Shengelaya, A., Bukowski, Z., Luetkens, H., Khasanov, R., Karpinski, J. and Keller, H. Muon-spin rotation measurements of the magnetic penetration depth in the Fe-based superconductor $\text{Ba}_{1-x}\text{Rb}_x\text{Fe}_2\text{As}_2$. *Phys. Rev. B* **84**, 094513 (2011).
- [4] Terashima, K., Sekiba, Y., Bowen, J.H., Nakayama, K., Kawahara, T., Sato, T., Richard, P., Xu, Y.M., Li, L.J., Cao, G.H., Xu, Z.A., Ding, H. and T. Takahashi, T. Fermi surface nesting induced strong pairing in iron-based superconductors. *Proc. Natl Acad. Sci. USA* **106**, 7330-7333 (2009).
- [5] Zhang, Y., Yang, L.X., Xu, M., Ye, Z.R., Chen, F., He, C., Xu, H.C., Jiang, J., Xie, B.P., Ying,

- J.J., Wang, X.F., Chen, X.H., Hu, J.P., Matsunami, M., Kimura, S. and Feng, D.L. Nodeless superconducting gap in $A_x\text{Fe}_2\text{Se}_2$ ($A = \text{K}, \text{Cs}$) revealed by angle-resolved photoemission spectroscopy. *Nature Mater.* **10**, 273-277 (2011).
- [6] Miao, H., Richard, P., Tanaka, Y., Nakayama, K., Qian, T., Umezawa, K., Sato, T., Xu, Y.-M., Shi, Y.-B., Xu, N., Wang, X.-P., Zhang, P., Yang, H.-B., Xu, Z.-J., Wen, J. S., Gu, G.-D., Dai, X., Hu, J.-P., Takahashi, T. and Ding, H. Isotropic superconducting gaps with enhanced pairing on electron Fermi surfaces in $\text{FeTe}_{0.55}\text{Se}_{0.45}$. *Phys. Rev. B* **85**, 094506 (2012).
- [7] Abdel-Hafeez, M., He, Z., Zhao, J., Lu, X., Luo, H., Dai, P. and Chen, X.-J. Crossover of the pairing symmetry from s - to d -wave in iron pnictide superconductors. Preprint at <http://arxiv.org/abs/1502.07130v1> (2015).
- [8] Biswas, P.K., Balakrishnan, G., Paul, D.M., Tomy, C.V., Lees, M.R. and Hillier, A.D. Muon-spin-spectroscopy study of the penetration depth of $\text{FeTe}_{0.5}\text{Se}_{0.5}$. *Phys. Rev. B* **81**, 092510 (2010).
- [9] Fletcher, J. D., Serafin, A., Malone, L., Analytis, J. G., Chu, J.-H., Erickson, A. S., Fisher, I. R. and Carrington, A. Evidence for a nodal-line superconducting state in LaFePO . *Phys. Rev. Lett.* **102**, 147001 (2009).
- [10] Hashimoto, K., Yamashita, M., Kasahara, S., Senshu, Y., Nakata, N., Tonegawa, S., Ikeda, K., Serafin, A., Carrington, A., Terashima, T., Ikeda, H., Shibauchi, T. and Matsuda, Y. Line nodes in the energy gap of superconducting $\text{BaFe}_2(\text{As}_{1-x}\text{P}_x)_2$ single crystals as seen via penetration depth and thermal conductivity. *Phys. Rev. B* **81**, 220501 (2010).
- [11] Yamashita, M., Senshu, Y., Shibauchi, T., Kasahara, S., Hashimoto, K., Watanabe, D., Ikeda, H., Terashima, T., Vekhter, I., Vorontsov, A. B. and Matsuda, Y. Nodal gap structure of superconducting $\text{BaFe}_2(\text{As}_{1-x}\text{P}_x)_2$ from angle-resolved thermal conductivity in a magnetic field. *Phys. Rev. B* **84**, 060507 (2011).
- [12] Nakai, Y., Iye, T., Kitagawa, S., Ishida, K., Kasahara, S., Shibauchi, T., Matsuda, Y. and Terashima, T. ^{31}P and ^{75}As NMR evidence for a residual density of states at zero energy in superconducting $\text{BaFe}_2(\text{As}_{0.67}\text{P}_{0.33})_2$. *Phys. Rev. B* **81**, 020503 (2010).
- [13] Hashimoto, K., Kasahara, S., Katsumata, R., Mizukami, Y., Yamashita, M., Ikeda, H., Terashima, T., Carrington, A., Matsuda, Y. and Shibauchi, T. Nodeless vs nodal order parameters in LiFeAs and LiFeP superconductors. *Phys. Rev. Lett.* **108**, 047003 (2012).
- [14] Dong, J. K., Zhou, S. Y., Guan, T. Y., Zhang, H., Dai, Y. F., Qiu, X., Wang, X. F., He, Y.,

- Chen, X. H. and Li, S. Y. Quantum criticality and nodal superconductivity in the FeAs-based superconductor KFe_2As_2 . *Phys. Rev. Lett.* **104**, 087005 (2010).
- [15] Qiu, X., Zhou, S. Y., Zhang, H., Pan, B. Y., Hong, X. C., Dai, Y. F., Eom, M.J., Kim, J. S. and Li, S. Y. Nodal superconductivity in $\text{Ba}(\text{Fe}_{1-x}\text{Ru}_x)_2\text{As}_2$ induced by isovalent Ru substitution. *Physical Review X* **2**, 011010 (2012).
- [16] Song, C.-L., Wang, Y.-L., Cheng, P., Jiang, Y.-P., Li, W., Zhang, T., Li, Z., He, K., Wang, L., Jia, J.-F., Hung, H.-H., Wu, C., Ma, X., Chen, X. and Xue Q.-K. Direct observation of nodes and twofold symmetry in FeSe superconductor. *Science* **332**, 1410-1413 (2010).
- [17] Zhang, Y., Ye, Z. R., Ge, Q. Q., Chen, F., Jiang, J., Xu, M., Xie, B. P. and Feng, D. L. Nodal superconducting-gap structure in ferropnictide superconductor $\text{BaFe}_2(\text{As}_{0.7}\text{P}_{0.3})_2$. *Nature Physics* **8**, 371-375 (2012).
- [18] Kuroki, K., Usui, H., Onari, S., Arita, R. and Aoki, H. Pnictogen height as a possible switch between high- T_c nodeless and low- T_c nodal pairings in the iron-based superconductors. *Phys. Rev. B* **79**, 224511 (2009).
- [19] Graser, S., Kemper, A. F., Maier, T. A., Cheng, H.-P., Hirschfeld, P. J. and Scalapino, D. J. *Phys. Rev. B* **81**, 214503 (2010).
- [20] Maiti, S., Korshunov, M. M., Maier, T. A. , Hirschfeld, P. J. and Chubukov, A. V. *Phys. Rev. Lett.* **107**, 147002 (2011).
- [21] Thomale, R., Platt, C., Hanke, W., Hu, J. and Bernevig, B.A. *Phys. Rev. Lett.* **107**, 117001 (2011).
- [22] Khodas, M. and Chubukov, A. V. *Phys. Rev. Lett.* **108**, 247003 (2012).
- [23] Fernandes, R. M., and Millis, A. J. *Phys. Rev. Lett.* **110**, 117004 (2013).
- [24] Kang, J., Kemper, A.F. and Fernandes, R. M. Manipulation of Gap Nodes by Uniaxial Strain in Iron-Based Superconductors. *Phys. Rev. Lett.* **113**, 217001 (2014).
- [25] Kretzschmar, F., Muschler, B., Böhm, T., Baum, A., Hackl, R., Wen, H.-H., Tsurkan, V., Deisenhofer, J. and Loidl, A. *Phys. Rev. Lett.* **110**, 187002 (2013).
- [26] Böhm, T. , Kemper, A.F., Moritz, B., Kretzschmar, F., Muschler, B., Eiter, H.-M., Hackl, R., Devereaux, T.P., Scalapino, D.J. and Wen, H.-H. A balancing act: Evidence for a strong subdominant d -wave pairing channel in $\text{Ba}_{0.6}\text{K}_{0.4}\text{Fe}_2\text{As}_2$. Preprint at <http://arxiv.org/abs/arXiv:1409.6815v1> (2014).
- [27] Tafti, F. F., Juneau-Fecteau, A., Delage, M. A., Cotret, S., Reid, J-Ph., Wang, A. F., Luo,

- X-G., Chen, X. H., Doiron-Leyraud, N. and Taillefer, L. Sudden reversal in the pressure dependence of T_c in the iron-based superconductor KFe_2As_2 . *Nat. Phys.* **9**, 349 (2013).
- [28] Sonier, J.E., Brewer, J.H. and Kiefl, R.F. *Rev. Mod. Phys.* **72**, 769 (2000).
- [29] Evtushinsky, D.V., Inosov, D.S., Zabolotnyy, V.B., Viazovska, M.S., Khasanov, R., Amato, A., Klauss, H.-H., Luetkens, H., Niedermayer, Ch., Sun, G.L., Hinkov, V., Lin, C.T., Varykhalov, A., Koitzsch, A., Knupfer, M., Büchner, B., Kordyuk, A.A. and Borisenko, S.V. Momentum-resolved superconducting gap in the bulk of $\text{Ba}_{1-x}\text{K}_x\text{Fe}_2\text{As}_2$ from combined ARPES and μSR measurements. *New J. Phys.* **11**, 055069 (2009).
- [30] Zabolotnyy, V.B., Evtushinsky, D.V., Kordyuk, A.A., Inosov, D.S., Koitzsch, A., Boris, A.V., Sun, G.L., Lin, C.T., Knupfer, M., Büchner, B., Varykhalov, A., Follath, R. and Borisenko, S.V. (π, π) electronic order in iron arsenide superconductors. *Nature* **457**, 569 (2009).
- [31] Hashimoto, K., Cho, K., Shibauchi, T., Kasahara, S., Mizukami, Y., Katsumata, R., Tsuruhara, Y., Terashima, T., Ikeda, H., Tanatar, M. A., Kitano, H., Salovich, N., Giannetta, R.W., Walmsley, P., Carrington, A., Prozorov, R. and Matsuda, Y. A Sharp Peak of the Zero-Temperature Penetration Depth at Optimal Composition in $\text{BaFe}_2(\text{As}_{1-x}\text{P}_x)_2$. *Science* **336**, 1554 (2012).
- [32] Wang, Y., Kreisel, A., Hirschfeld, P. J. and Mishra, V. *Phys. Rev. B* **87**, 094504 (2013).
- [33] Sonier, J.E., Huang, W., Kaiser, C.V., Cochrane, C., Pacradouni, V., Sabok-Sayr, S.A., Lumsden, M.D., Sales, B.C., McGuire, M.A., Sefat, A.S. and Mandrus, D. Magnetism and Disorder Effects on Muon Spin Rotation Measurements of the Magnetic Penetration Depth in Iron-Arsenic Superconductors. *Phys. Rev. Lett.* **106**, 127002 (2011).
- [34] Brandt, E.H. Flux distribution and penetration depth measured by muon spin rotation in high- T_c superconductors. *Phys. Rev. B* **37**, 2349 (1988).
- [35] Suter, A. and Wojek, B.M. *Physics Procedia* **30**, 69 (2012).
- The fitting of the T -dependence of the penetration depth with α model was performed using the additional library BMW developped by B.M. Wojek.
- [36] Tinkham, M. Introduction to Superconductivity, *Krieger Publishing Company, Malabar, Florida*, 1975.
- [37] Carrington, A. and Manzano, F. Magnetic penetration depth of MgB_2 . *Physica C* **385**, 205 (2003).
- [38] Fang, M.H., Pham, H.M., Qian, B., Liu, T.J., Vehstedt, E.K., Liu, Y., Spinu, L. and Mao,

- Z.Q. Superconductivity close to magnetic instability in $\text{Fe}(\text{Se}_{1-x}\text{Te}_x)_{0.82}$. *Phys. Rev. B* **78**, 224503 (2008).
- [39] Padamsee, H., Neighbor, J.E. and Shiffman, C.A. Quasiparticle Phenomenology for Thermodynamics of Strong-Coupling Superconductors. *J. Low Temp. Phys.* **12**, 387 (1973).
- [40] Khasanov, R., Shengelaya, A., Maisuradze, A., La Mattina, F., Bussmann-Holder, A., Keller, H. and Müller, K. A. Experimental Evidence for Two Gaps in the High-Temperature $\text{La}_{1.83}\text{Sr}_{0.17}\text{CuO}_4$ Superconductor. *Phys. Rev. Lett.* **98**, 057007 (2007).
- [41] Fernandes, R. M. and Schmalian, J. *Phys. Rev. B* **84**, 012505 (2011).
- [42] Stanev, V., Alexandrov, B. S., Nikolic, P. and Tesanovic, Z. *Phys. Rev. B* **84**, 014505 (2011).
- [43] Fernandes, R. M. and Millis, A. J. *Phys. Rev. Lett.* **111**, 127001 (2013).
- [44] Hashimoto, K., Kasahara, S., Katsumata, R., Mizukami, Y., Yamashita, M., Ikeda, H., Terashima, T., Carrington, A., Matsuda, Y. and Shibauchi, T. Nodal versus Nodeless Behaviors of the Order Parameters of LiFeP and LiFeAs Superconductors from Magnetic Penetration-Depth Measurements. *Phys. Rev. Lett.* **108**, 047003 (2012).
- [45] Walmsley, P., Putzke, C., Malone, L., Guillamon, I., Vignolles, D., Proust, C., Badoux, S., Coldea, A.I., Watson, M.D., Kasahara, S., Mizukami, Y., Shibauchi, T., Matsuda, Y. and Carrington, A. Quasiparticle Mass Enhancement Close to the Quantum Critical Point in $\text{BaFe}_2(\text{As}_{1-x}\text{P}_x)_2$. *Phys. Rev. Lett.* **110**, 257002 (2013).
- [46] Levchenko, A., Vavilov, M.G., Khodas, M. and Chubukov, A.V. *Phys. Rev. Lett.* **110**, 177003 (2013).
- [47] Chowdhury, D., Swingle, B., Berg, E. and Sachdev, S. Singularity of the London Penetration Depth at Quantum Critical Points in Superconductors. *Phys. Rev. Lett.* **111**, 157004 (2013).
- [48] Prando, G., Hartmann, Th., Schottenhamel, W., Guguchia, Z., Sanna, S., Ahn, F., Nekrasov, I., Wolter, A. U. B., Wurmehl, S., Khasanov, R., Eremin, I. and Büchner, B. Mutual independence of critical temperature and superfluid density under pressure in optimally electron-doped superconducting $\text{LaFeAsO}_{1-x}\text{F}_x$. Preprint at <http://arxiv.org/abs/arXiv:1502.02713> (2015).
- [49] Maisuradze, A., Graneli, B., Guguchia, Z., Shengelaya, A., Pomjakushina, E., Conder, K. and Keller, H. Effect of pressure on the Cu and Pr magnetism in $\text{Nd}_{1-x}\text{Pr}_x\text{Ba}_2\text{Cu}_3\text{O}_7$ investigated by muon spin rotation. *Phys. Rev. B* **87**, 054401 (2013).
- [50] Andreica, D. 2001 *Ph.D. thesis* IPP/ETH-Zürich.
- [51] Maisuradze, A., Shengelaya, A., Amato, A., Pomjakushina, E. and Keller, H. Muon spin

rotation investigation of the pressure effect on the magnetic penetration depth in $\text{YBa}_2\text{Cu}_3\text{O}_x$.
Phys. Rev. B **84**, 184523 (2011).

SUPPLEMENTAL MATERIAL

A. Experimental Details

1. Sample characterization

The temperature dependence of the zero field-cooled (ZFC) and field-cooled (FC) diamagnetic susceptibility of $\text{Ba}_{0.65}\text{Rb}_{0.35}\text{Fe}_2\text{As}_2$ measured in a magnetic field of $\mu_0 H = 1 \text{ mT}$ is shown in Fig. 6(a). From the diamagnetic response the SC transition temperature T_c is de-

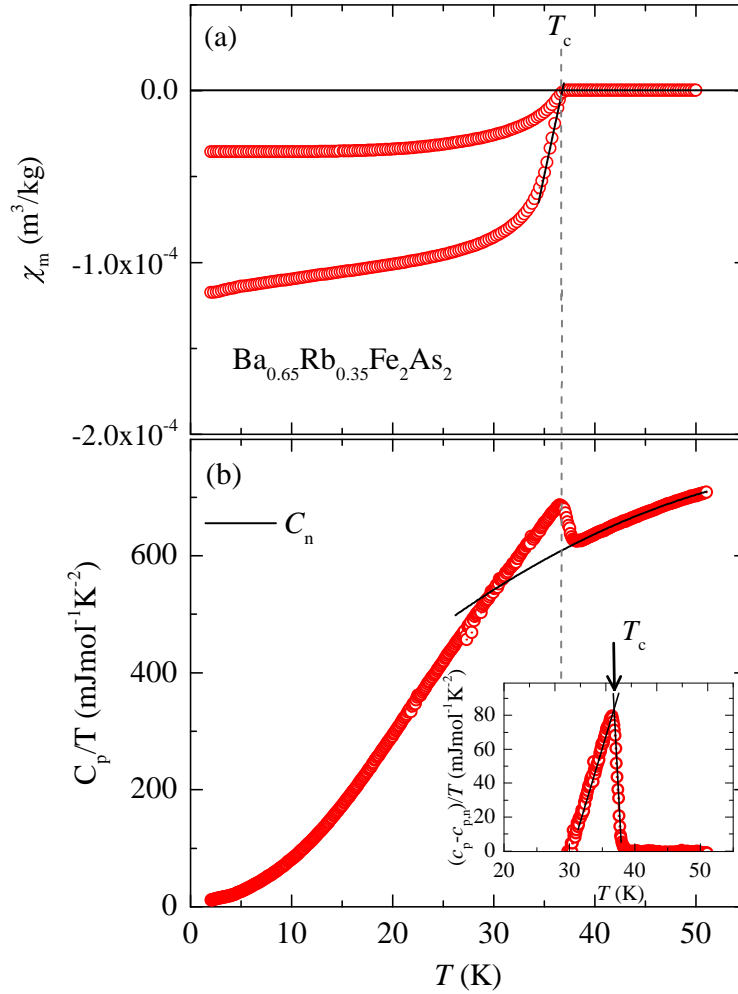


Figure 6: (Color online) (a) Temperature dependence of the zero-field cooled (ZFC) and field-cooled (FC) susceptibility χ_m obtained in an applied magnetic field of $\mu_0 H = 10 \text{ mT}$ for optimally doped $\text{Ba}_{0.65}\text{Rb}_{0.35}\text{Fe}_2\text{As}_2$. (b) Specific heat C_p/T as a function of temperature of $\text{Ba}_{0.65}\text{Rb}_{0.35}\text{Fe}_2\text{As}_2$. The arrow denotes the superconducting transition temperature T_c .

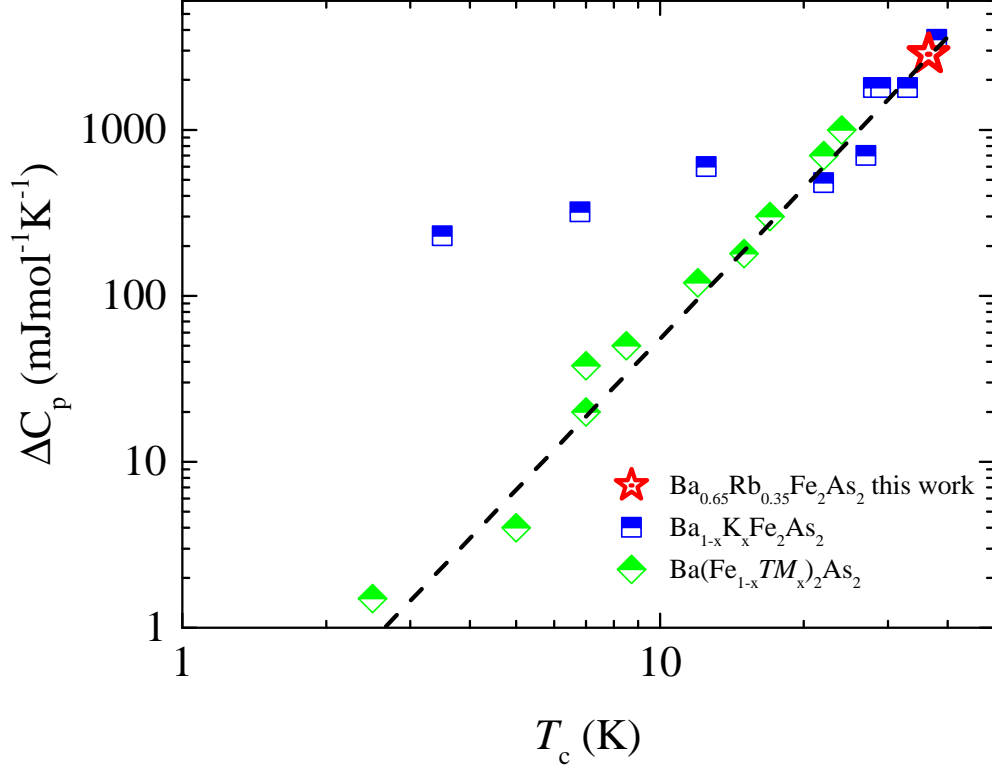


Figure 7: (Color online) (a) Specific heat jump ΔC_p at the superconducting transition vs T_c for $\text{Ba}_{0.65}\text{Rb}_{0.35}\text{Fe}_2\text{As}_2$, plotted together with literature data for various FeAs-based superconductors. The line corresponds to $\Delta C_p \propto T^3$ (after [1]).

terminated from the intercept of the linearly extrapolated zero-field cooled (ZFC) susceptibility curve with $\chi_m = 0$ line, and it is found to be $T_c = 36.8(5)$ K. The temperature-dependent heat capacity data for this sample plotted as C_p/T vs T is shown in Fig. 6(b). The jump associated with the SC transitions is clearly seen. Here the anomaly at the transition has been isolated from the phonon dominated background by subtracting a second order polynomial $C_{p,n}$ fitted above T_c and extrapolated to lower temperature. The quantity $\Delta C_p/T$ with $\Delta C_p = (C_p - C_{p,n})$ is presented as a function of temperature in the inset of Fig. 6(b). Although there may be some uncertainty in using this procedure over an extended temperature range, the lack of appreciable thermal SC fluctuations, as evidenced by the mean-field-like form of the anomaly, means that there is very little uncertainty in the size of ΔC_p . Bud'ko et. al. [1] found that in many '122' Fe-based superconductors the specific heat jump ΔC_p at T_c follows the empirical trend, the so-called BNC scaling $\Delta C_p \propto T^3$. This has been interpreted as either originating from quantum critically or from strong impurity pair breaking. A violation

of the BNC scaling was observed for $\text{Ba}_{1-x}\text{K}_x\text{Fe}_2\text{As}_2$ for $x > 0.7$ [1] and in addition a change of the SC gap symmetry was observed. The specific heat jump data for $\text{Ba}_{0.65}\text{Rb}_{0.35}\text{Fe}_2\text{As}_2$ obtained in this work is added in Fig. 7 to the BNC plot taken from Ref. [1]. Our data point lies perfectly on the BNC line.

2. Muon spin rotation experiments

Zero-field (ZF) and transverse-field (TF) μSR experiments at ambient and under various applied pressures were performed at the μE1 beamline of the Paul Scherrer Institute (PSI), Switzerland, using the dedicated GPD spectrometer. A gas-flow ^4He (base temperature ~ 4 K) and a VARIOX cryostat (base temperature ~ 1.3 K) were used. High energy muons ($p_{\hat{f}\frac{1}{4}} = 100$ MeV/c) were implanted in the sample. Forward and backward positron detectors with respect to the initial muon spin polarization were used for the measurements of the μSR asymmetry time spectrum $A(t)$. The typical statistics for both forward and backward detectors were 6 millions. All ZF and TF μSR experiments were performed by stabilizing the temperature in prior to recording the μSR -time spectra. Note that a precise calibration of the GPD results was carried out at the πM3 beamline using the low background general purpose instrument (GPS). The μSR time spectra were analyzed using the free software package MUSRFIT [2].

In a μSR experiment nearly 100 % spin-polarized muons μ^+ are implanted into the sample one at a time. The positively charged μ^+ thermalize at interstitial lattice sites, where they act as magnetic microprobes. In a magnetic material the muon spin precesses either in the local or applied magnetic field B_μ at the penetration depth λ and the coherence length ξ . If a type II superconductor is cooled below T_c in an applied magnetic field ranged between the lower (H_{c1}) and the upper (H_{c2}) critical fields, a vortex lattice is formed which in general is incommensurate with the crystal lattice and the vortex cores will be separated by much larger distances than those of the unit cell. Because the implanted muons stop at given crystallographic sites, they will randomly probe the field distribution of the vortex lattice. Such measurements need to be performed in a field applied perpendicular to the initial muon spin polarization (so called TF configuration).

3. Results of the Zero-Field μ SR experiments

It is well known that undoped BaFe_2As_2 is not superconducting at ambient pressure and undergoes a spin-density wave (SDW) transition of the Fe-moments far above T_c [3]. The SC state can be achieved either under pressure [4, 5] or by appropriate charge carrier doping of the parent compound [6], leading to a suppression of the SDW state. Magnetism, if present in the samples, must be taken into account in the TF- μ SR data analysis. Therefore, we have carried out ZF- μ SR experiments above and below T_c to search for magnetism in $\text{Ba}_{0.65}\text{Rb}_{0.35}\text{Fe}_2\text{As}_2$. As an example, ZF- μ SR spectra recorded at $T=5$ K and 50 K of $\text{Ba}_{0.65}\text{Rb}_{0.35}\text{Fe}_2\text{As}_2$ are shown in Fig. 8a. There is no precession signal, indicating that there is no long-range magnetic order. On the other hand, we observed a significant drop of the asymmetry, taking place within $0.2 \mu\text{s}$. This is caused by the presence of diluted Fe moments as discussed in previous μ SR studies [7]. In order to quantify the magnetic fraction, the ZF- μ SR data were analyzed by the following function:

$$A_{ZF}(t) = \Omega A_0 \left[\frac{2}{3} e^{-\lambda_T t} + \frac{1}{3} e^{-\lambda_L t} \right] + (1 - \Omega) A_0 \left[\frac{1}{3} + \frac{2}{3} (1 - \sigma^2 t^2 - \Lambda t) e^{(-\frac{\sigma^2 t^2}{2} - \Lambda t)} \right]. \quad (4)$$

the first and the second terms describe the magnetic and nonmagnetic part of the signals, respectively. A_0 is the initial asymmetry, Ω is the magnetic volume fraction, and λ_T (λ_L) is

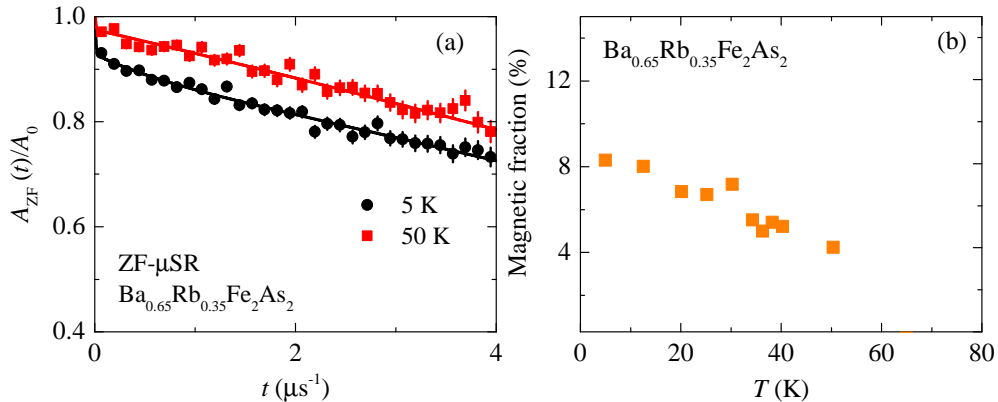


Figure 8: (Color online) (a) The ZF- μ SR time spectra for $\text{Ba}_{0.65}\text{Rb}_{0.35}\text{Fe}_2\text{As}_2$ recorded above and below T_c . The solid line represent the fits to the data by means of Eq. (1). (b) Temperature dependence of the magnetic fraction of $\text{Ba}_{0.65}\text{Rb}_{0.35}\text{Fe}_2\text{As}_2$, extracted from the ZF- μ SR experiments.

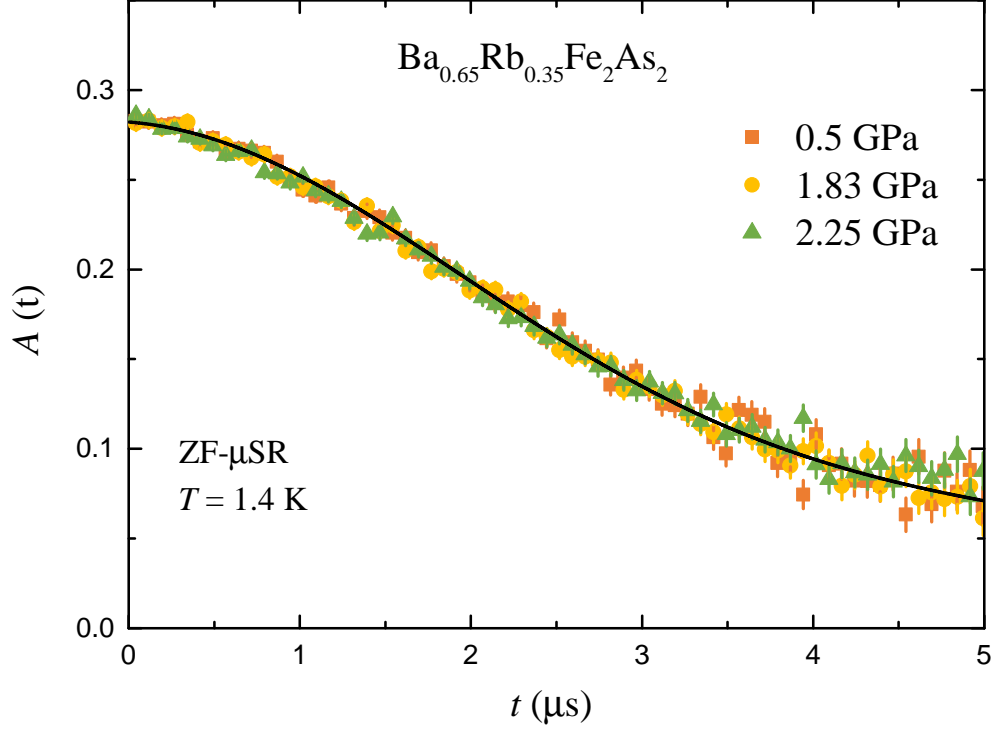


Figure 9: (Color online) ZF- μ SR time spectra for $\text{Ba}_{0.65}\text{Rb}_{0.35}\text{Fe}_2\text{As}_2$ at various applied pressures recorded at the base temperature $T = 1.4 \text{ K}$. The solid line represents the fit to the data by means of the sum of the Eq. (1) and a damped Kubo-Toyabe depolarization function to account for the pressure cell signal.

the transverse (longitudinal) depolarization rate of the μ SR signal, arising from the magnetic part of the sample. The second term describing the paramagnetic part of the sample is the combination of a Lorentzian and a Gaussian Kubo-Toyabe depolarization functions [8, 9]. σ and Λ are the depolarization rates due to the nuclear dipole moments and randomly oriented diluted local electronic moments, respectively. The temperature dependence of the magnetic fraction obtained for $\text{Ba}_{0.65}\text{Rb}_{0.35}\text{Fe}_2\text{As}_2$ is plotted in Fig. 8b. The magnetic fraction at the base temperature was found to be only 8 %. Bearing in mind that the signal from the magnetically ordered parts vanishes within the first $0.2 \mu\text{s}$ in the whole temperature region, the analysis of transverse field data was restricted to times $t > 0.2 \mu\text{s}$.

Figure 9 shows the ZF- μ SR time spectra for $\text{Ba}_{0.65}\text{Rb}_{0.35}\text{Fe}_2\text{As}_2$ at various applied pressures. The ZF relaxation rate stays nearly unchanged between $p = 0 \text{ GPa}$ and 2.25 GPa , implying that there is no sign of pressure induced magnetism in this system.

B. Microscopic model for analyzing the penetration depth data of $\text{Ba}_{0.65}\text{Rb}_{0.35}\text{Fe}_2\text{As}_2$

1. Model for s^{+-} pairing

As a minimal model that accounts for the different superconducting states of the iron pnictides (nodeless s^{+-} , nodal s^{+-} , and d -wave), we consider a two-dimensional system with three isotropic Fermi pockets [10]: one hole pocket h centered around $\Gamma = (0, 0)$ and two electron pockets e_1 and e_2 centered around $M_1 = (\pi, 0)$ and $M_2 = (0, \pi)$ (see Fig. 10). To describe the s^{+-} state, the pairing interaction between the hole pocket h and the electron pocket e_1 is assumed to be angular dependent with the form:

$$V_{he_1} = V_0(r - \cos 2\phi)h_{\uparrow}^{\dagger}(\mathbf{k})h_{\downarrow}^{\dagger}(-\mathbf{k})e_{1\downarrow}(-\mathbf{p})e_{1\uparrow}(\mathbf{p}) + h.c. , \quad (5)$$

where ϕ is the polar angle measured relative to the center of the electron pocket, V_0 is the interaction energy scale, and r is the relative amplitude of the angular-independent and the angular-dependent pairing interactions. Due to the tetragonal symmetry of the system, the pairing interaction between h and e_2 is:

$$V_{he_2} = V_0(r + \cos 2\phi)h_{\uparrow}^{\dagger}(\mathbf{k})h_{\downarrow}^{\dagger}(-\mathbf{k})e_{2\downarrow}(-\mathbf{p})e_{2\uparrow}(\mathbf{p}) + h.c. . \quad (6)$$

Furthermore, to minimize the number of free parameters, we assume that the three pockets have the same Fermi velocity v_f , while the density of states can in principle be different $\rho_h/\rho_e = \eta$. Within this model, we obtain an s^{+-} state, where the SC gap of the hole pocket is a constant, Δ_h , and the gap on the electron pockets is of the form $\Delta_{e_1} = \Delta_e(r - \cos 2\phi)$ and $\Delta_{e_2} = \Delta_e(r + \cos 2\phi)$. Accidental nodes appear in the electron pockets if $r < 1$. Introducing the energy cutoff Λ_c , we can write down the corresponding BCS-like gap equations:

$$\begin{aligned} \Delta_h &= -\rho_e V_0 \Delta_e \int_{-\Lambda_c}^{\Lambda_c} d\epsilon \int \frac{d\phi}{2\pi} \left(\frac{(r + \cos 2\phi)^2}{2E_{e_1}(\mathbf{k})} \tanh \frac{\beta E_{e_1}(\mathbf{k})}{2} + \frac{(r - \cos 2\phi)^2}{2E_{e_2}(\mathbf{k})} \tanh \frac{\beta E_{e_2}(\mathbf{k})}{2} \right) \\ \Delta_e &= -\rho_h V_0 \Delta_h \int_{-\Lambda_c}^{\Lambda_c} \frac{d\epsilon}{2E_h(\mathbf{k})} \tanh \frac{\beta E_h(\mathbf{k})}{2} \end{aligned} \quad (8)$$

where $E_{e_1}(\mathbf{k})$, $E_{e_2}(\mathbf{k})$, and $E_h(\mathbf{k})$ are the quasi-particle energy dispersions:

$$E_{e_1}(\mathbf{k}) = \sqrt{\epsilon_e^2 + \Delta_e^2(r - \cos 2\phi)^2}, \quad E_{e_2}(\mathbf{k}) = \sqrt{\epsilon_e^2 + \Delta_e^2(r + \cos 2\phi)^2}, \quad E_h(\mathbf{k}) = \sqrt{\epsilon_h^2 + \Delta_h^2}.$$

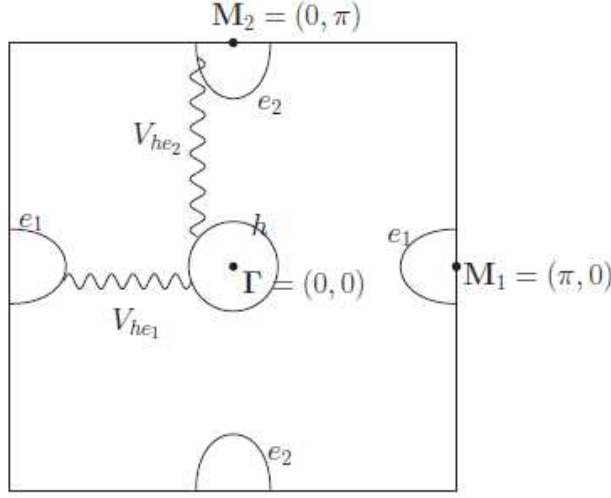


Figure 10: (Color online) Three pocket model used in our calculations. It is assumed that the system has one hole pocket h centered around $\Gamma = (0, 0)$ and two electron pockets e_1 and e_2 centered around $M_1 = (\pi, 0)$ and $M_2 = (0, \pi)$.

To determine T_c , we linearize the gap equations, yielding:

$$\begin{cases} \Delta_h = -\Delta_e \rho_e V_0 (2r^2 + 1) \int_0^{\Lambda_c} \frac{d\epsilon}{\epsilon} \tanh \frac{\beta_c \epsilon}{2} \\ \Delta_e = -\Delta_h \eta \rho_e V_0 \int_0^{\Lambda_c} \frac{d\epsilon}{\epsilon} \tanh \frac{\beta_c \epsilon}{2} \end{cases} \implies \rho_e V_0 = \left[\sqrt{\eta(2r^2 + 1)} \int_0^{\Lambda_c} \frac{d\epsilon}{\epsilon} \tanh \frac{\beta_c \epsilon}{2} \right]^{-1}$$

To perform the fitting, we set T_c to be fixed, and set the energy cutoff $\Lambda_c = 86\text{meV}$ (the results do not depend significantly on the choice of the cutoff). This provides a constraint on $\rho_e V_0$, η , and r . When $T < T_c$, the gaps are calculated based on the BCS Eqs. (7) and (8).

The expression for the penetration depth of a single-band system is:

$$\lambda_{\mu\mu}^{-2}(T) = \frac{4\pi}{cV} \sum_{\mathbf{k}} \left[\left\langle \frac{\partial^2 \epsilon}{\partial k_\mu^2} \right\rangle + \left(\frac{\partial \epsilon}{\partial k_\mu} \right)^2 \frac{\partial f}{\partial E_k} \right] \rightarrow \frac{1}{V} \sum_{\mathbf{k}} \left(\frac{\partial \epsilon}{\partial k_\mu} \right)^2 \left[\frac{\partial f}{\partial E_k} - \frac{\partial f}{\partial \epsilon_k} \right],$$

where f is the Fermi distribution function, ϵ is the energy of the non-interacting system, and E_k is the quasi-particle energy dispersion. Applying this formula to our three pocket

model, we obtain

$$\begin{aligned}
\lambda^{-2}(T) &\propto \rho_h \frac{v_f^2}{2} \int_{-\Lambda_c}^{\Lambda_c} d\epsilon \left(\frac{\partial f}{\partial E_h} - \frac{\partial f}{\partial \epsilon_h} \right) + \rho_e v_f^2 \int_{-\Lambda_c}^{\Lambda_c} d\epsilon \int \frac{d\phi}{2\pi} \cos^2 \phi \left(\frac{\partial f}{\partial E_{e_1}} - \frac{\partial f}{\partial \epsilon_e} \right) \\
&\quad + \rho_e v_f^2 \int_{-\Lambda_c}^{\Lambda_c} d\epsilon \int \frac{d\phi}{2\pi} \cos^2 \phi \left(\frac{\partial f}{\partial E_{e_2}} - \frac{\partial f}{\partial \epsilon_e} \right) \\
\lambda^{-2}(T) &\propto \rho_e v_f^2 \left[\frac{2+\eta}{2} (1 - 2f(\Lambda_c)) + \eta \int_0^{\Lambda_c} d\epsilon \frac{\partial f}{\partial E_h} + 2 \int_0^{\Lambda_c} d\epsilon \int \frac{d\phi}{2\pi} \frac{\partial f}{\partial E_e} \right] \quad (9)
\end{aligned}$$

In the fittings, we will focus on the normalized penetration depth $\lambda^{-2}(T)/\lambda^{-2}(0)$.

2. Model for *d*-wave pairing

To describe the *d*-wave superconducting state within our three band model, we consider the following form of the pairing interaction:

$$\begin{aligned}
V_{he_1} &= V_0(r - \cos 2\theta) h_{\uparrow}^{\dagger}(\mathbf{k}) h_{\downarrow}^{\dagger}(-\mathbf{k}) e_{1\downarrow}(-\mathbf{p}) e_{1\uparrow}(\mathbf{p}) + h.c. \\
V_{he_2} &= V_0(r + \cos 2\theta) h_{\uparrow}^{\dagger}(\mathbf{k}) h_{\downarrow}^{\dagger}(-\mathbf{k}) e_{2\downarrow}(-\mathbf{p}) e_{2\uparrow}(\mathbf{p}) + h.c. .
\end{aligned}$$

where θ is the angle around the hole pocket. The gap functions can then be written as:

$$\Delta_{e_1} = -\Delta_{e_2} = \Delta_e, \quad \Delta_h(\mathbf{k}) = \Delta_h \cos 2\theta.$$

resulting in the BCS-like gap equations:

$$\begin{aligned}
\Delta_h &= 2\Delta_e \rho_e V_0 \int_{-\Lambda_c}^{\Lambda_c} \frac{d\epsilon}{2E_e} \tanh \frac{\beta E_e}{2} \\
\Delta_e &= \Delta_h \eta \rho_e V_0 \int_{-\Lambda_c}^{\Lambda_c} d\epsilon \int \frac{d\theta}{2\pi} \frac{\cos^2 2\theta}{2E_h} \tanh \frac{\beta E_h}{2}
\end{aligned}$$

Here, $\eta = \rho_h/\rho_e$, $E_e = \sqrt{\epsilon_e^2 + \Delta_e^2}$, and $E_h = \sqrt{\epsilon^2 + \Delta_h^2 \cos^2 2\theta}$. Repeating the same steps as for the s^{+-} case, we obtain the penetration depth:

$$\lambda^{-2}(T) \propto \rho_e v_f^2 \left[\frac{2+\eta}{2} (1 - 2f(\Lambda_c)) + \eta \int_0^{\Lambda_c} d\epsilon \int \frac{d\theta}{2\pi} \frac{\partial f}{\partial E_h} + 2 \int_0^{\Lambda_c} d\epsilon \frac{\partial f}{\partial E_e} \right] \quad (10)$$

Comparing the expressions for the *d*-wave case to the expressions we derived for the s^{+-} case, Eqs. (7) and (9), we note that they can be mapped onto each other if $r = 0$. In this extreme case, changing $\eta_d \rightarrow 4/\eta_s$, $V_{0,d} \rightarrow \eta V_{0,s}/2$, and $\Delta_h \leftrightarrow \Delta_e$ leads to the same gap equations and penetration depth expression. With these replacements, both *s* and *d* pairing give the same $\lambda^{-2}(T)/\lambda^{-2}(0)$. Therefore, we conclude that the penetration depth cannot distinguish between nodal- s^{+-} and *d*-wave if the nodal- s^{+-} is the extreme case with $r = 0$.

3. Fitting Results

We now fit the experimental data $\lambda^{-2}(T)/\lambda^{-2}(0)$ of optimally-doped $\text{Ba}_{1-x}\text{Rb}_x\text{Fe}_2\text{As}_2$ to find the values of $\rho_e V_0$, η , and r for different pressures. Note that the value of T_c imposes another constraint on these three parameters, as explained above. Figs. 11a, b and c show the fitting for the s^{+-} model for $P = 0$, $P = 1.57$ GPa, and $P = 2.25$ GPa, respectively. For the $P = 0$ case, we find equal gap amplitudes and no nodes, as seen by ARPES experiments in the related compound $\text{Ba}_{1-x}\text{K}_x\text{Fe}_2\text{As}_2$. We see that the fitting is not as good in the region immediately below T_c . We will discuss this issue in more details below. For the pressurized samples, the fitting is overall better and indicates a nodal state ($r < 1$). The value of the density of states ratio ρ_h/ρ_e is little affected by pressure (as expected, since no charge carriers are introduced), and is consistent with the value of a nearly compensated metal.

Surprisingly, the best fittings for both the $P = 1.57$ GPa and $P = 2.25$ GPa cases give $r = 0$, where the nodes on the electron pockets are fixed at $\theta = \pm\pi/4$. This is a very special case of the accidentally nodal s^{+-} state, since by symmetry there is no reason for r to vanish. To make this point more transparent, in Fig. 12a we plot the non-zero pressure data and the theoretical curves for the penetration depth for various values of r – keeping all the other parameters constant. Clearly, $0 < r < 1$ gives worst fittings than $r = 0$. What

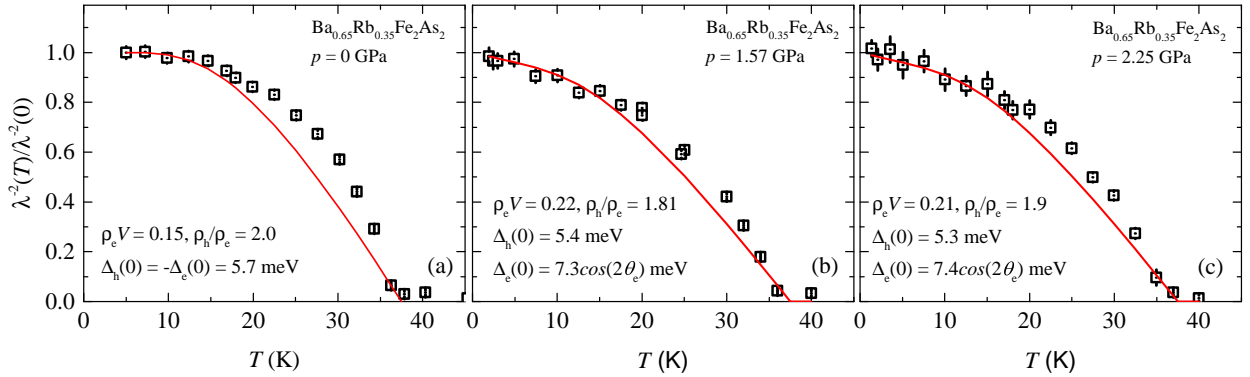


Figure 11: (Color online) The temperature dependence of $\lambda^{-2}(T)/\lambda^{-2}(0)$ measured at various applied hydrostatic pressures of $\text{Ba}_{0.65}\text{Rb}_{0.35}\text{Fe}_2\text{As}_2$. The square symbols are experimental data and the red curves are the theoretical functions. (a) Fitting for the $P = 0$ data, which suggests a nodeless state. (b) and (c) Fitting for $P = 1.57$ GPa and $P = 2.25$ GPa. The fitting suggests that nodes exist on the two electron pockets at the angles $\theta_e = \pm\pi/4$ and $\pm 3\pi/4$.

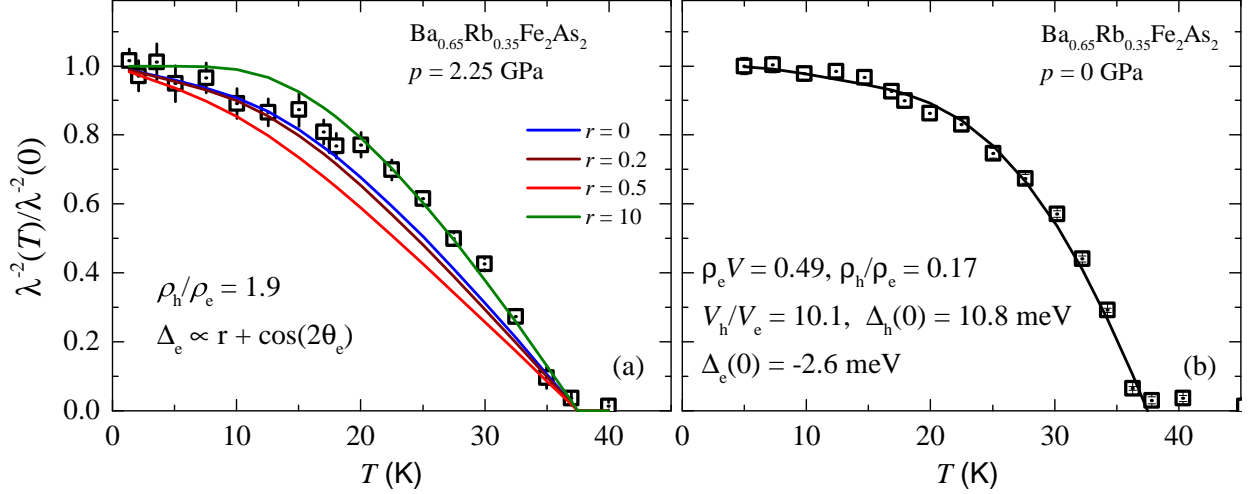


Figure 12: (Color online) (a) Effect of the electron pocket gap anisotropy on the penetration depth at $p = 2.25$ GPa. The electron gap is nodal if $r < 1$, and becomes nodeless if $r > 1$. The low temperature data clearly shows that the gap is nodal, but the data near T_c seems to be better described by a nodeless state. (b) Fitting for the zero pressure case with the Fermi velocity ratio v_h/v_e being a free parameter. The fitting improves with respect to Fig. 6a, but the values of v_h/v_e and ρ_h/ρ_e seem to be too large or too small.

we also found is that $r = 10$ – i.e. a nodeless superconducting state – describes the data better near T_c , on the expense of a very bad fitting at low temperatures – where the nodal behavior is evident.

As we discussed in the previous section, a nodal- s^{+-} state with $r = 0$ is indistinguishable – for fitting purposes – from a d -wave state. Since there is no symmetry reason to have $r = 0$ in our simple model, or even $r \ll 1$ over a wide pressure range, we interpret this result as an indirect indication that a d -wave state is more likely to be the state of the pressurized samples.

Finally, we comment on the difficulty of the fittings to capture the behavior near T_c – particularly for the sample at ambient pressure (see Fig. 11a). One reason could be the presence of inhomogeneities, which would require a distribution of gaps to be taken into account, instead of a single gap value. Another reason could be related to our choice of fixing the Fermi velocities to be the same for both the electron and hole pockets. To investigate this possibility, we lift this restriction and allow v_h/v_e to also be a fitting parameter. The result is shown in Fig. 12b. Clearly, we obtain a better fitting, but not only $\rho_e V_0$ is relatively large,

but the ratios ρ_h/ρ_e and v_h/v_e are very large or very small, which is difficult to reconcile with the Fermi surface of these materials. Most likely, additional pockets are necessary to capture the full temperature dependence of the penetration depth. Nevertheless, our microscopic model provides results that agree with those obtained from the α -model fitting, particularly in the low-temperature regime, suggesting that a d -wave state is more likely to be realized than a nodal s^{+-} state.

* Electronic address: zurab.guguchia@psi.ch

- [1] Sergey L. Bud'ko, Ni Ni, and Paul C. Canfield, Phys. Rev. B **79**, 220516(R) (2009).
- [2] A. Suter and B.M. Wojek, *Physics Procedia* **30**, 69-73 (2012).
- [3] Q. Huang, Y. Qiu, W. Bao, M.A. Green, J.W. Lynn, Y.C. Gasparovic, T. Wu, G. Wu, X.H. Chen, Phys. Rev. Lett. **101**, 257003 (2008).
- [4] M.S. Torikachvili, S.L. Bud'ko, N. Ni, and P.C. Canfield, Phys. Rev. Lett. **101**, 057006 (2008).
- [5] C.F. Miclea, M. Nicklas, H.S. Jeevan, D. Kasinathan, Z. Hossain, H. Rosner, P. Gegenwart, C. Geibel, and F. Steglich, Phys. Rev. B **79**, 212509 (2009).
- [6] J. Zhao, Q. Huang, C. de la Cruz, S. Li, J.W. Lynn, Y. Chen, M.A. Green, G.F. Chen, G. Li, Z. Li, J.L. Luo, N.L. Wang, and P. Dai, Nature Materials **7**, 953 (2008).
- [7] R. Khasanov, D.V. Evtushinsky, A. Amato, H.-H. Klauss, H. Luetkens, Ch. Niedermayer, B. Büchner, G.L. Sun, C.T. Lin, J.T. Park, D.S. Inosov, and V. Hinkov. Phys. Rev. Lett. **102**, 187005 (2009).
- [8] R. Kubo and T. Toyabe, *Magnetic Resonance and Relaxation* (North Holland, Amsterdam, 1967).
- [9] R.S. Hayano, Y.J. Uemura, J. Imazato, N. Nishida, T. Yamazaki, and R. Kubo, Phys. Rev. B **20**, 850 (1979).
- [10] Jian Kang, Alexander F. Kemper, and Rafael M. Fernandes. Phys. Rev. Lett. **113**, 217001 (2014).